

Article

Modeling the Inter-Arrival Time Between Severe Storms in the United States Using Finite Mixtures

Ilana Vinnik  and Tatjana Miljkovic * 

Department of Statistics, Miami University, Oxford, OH 45056, USA; vinniki@miamioh.edu

* Correspondence: miljkot@miamioh.edu

Abstract: When inter-arrival times between events follow an exponential distribution, this implies a Poisson frequency of events, as both models assume events occur independently and at a constant average rate. However, these assumptions are often violated in real-insurance applications. When the rate at which events occur changes over time, the exponential distribution becomes unsuitable. In this paper, we study the distribution of inter-arrival times of severe storms, which exhibit substantial variability, violating the assumption of a constant average rate. A new approach is proposed for modeling severe storm recurrence patterns using a finite mixture of log-normal distributions. This approach effectively captures both frequent, closely spaced storm events and extended quiet periods, addressing the inherent variability in inter-event durations. Parameter estimation is performed using the Expectation–Maximization algorithm, with model selection validated via the Bayesian information criterion (BIC). To complement the parametric approach, Kaplan–Meier survival analysis was employed to provide non-parametric insights into storm-free intervals. Additionally, a simulation-based framework estimates storm recurrence probabilities and assesses financial risks through probable maximum loss (PML) calculations. The proposed methodology is applied to the Billion-Dollar Weather and Climate Disasters dataset, compiled by the U.S. National Oceanic and Atmospheric Administration (NOAA). The results demonstrate the model’s effectiveness in predicting severe storm recurrence intervals, offering valuable tools for managing risk in the property and casualty insurance industry.



Academic Editor: Annamaria Olivieri

Received: 19 December 2024

Revised: 9 January 2025

Accepted: 13 January 2025

Published: 21 January 2025

Citation: Vinnik, Ilana, and Tatjana Miljkovic. 2025. Modeling the Inter-Arrival Time Between Severe Storms in the United States Using Finite Mixtures. *Risks* 13: 19. <https://doi.org/10.3390/risks13020019>

Copyright: © 2025 by the authors. Licensee MDPI, Basel, Switzerland. This article is an open access article distributed under the terms and conditions of the Creative Commons Attribution (CC BY) license (<https://creativecommons.org/licenses/by/4.0/>).

Keywords: EM algorithm; mixture models; Kaplan–Meier estimators; probable maximum loss; severe storms; United States

1. Introduction

In most risk assessment applications, the inter-arrival times between events (e.g., insurance claims) are often assumed to follow an exponential distribution as a consequence of a Poisson process. The Poisson process assumes that events occur independently within a fixed time interval at a constant average rate. Additionally, it assumes that events occur one at a time and that the probability of an event occurring in a small interval is proportional to the length of the interval (see [Kaas et al. 2008](#); [Klugman et al. 2019](#)). However, these assumptions are frequently violated in real-world insurance applications.

To illustrate the challenges of modeling inter-arrival times for risk assessment, this study focuses on the inter-arrival times between severe storms in the United States. Severe storms are among the most destructive natural events, with far-reaching impacts on life, infrastructure, and the economy. The Property and Casualty Insurance Industry in the U.S. is particularly concerned with the frequency and severity of these storms. According to a

report published by the National Association of Insurance Commissioners (NAIC 2023), insured losses from natural catastrophes in the United States totaled roughly USD 80 billion in 2023. The majority of these losses resulted from severe convective storms rather than isolated large-scale events like hurricanes.

Severe storms, which encompass high-impact weather phenomena such as hail, tornadoes, derechos, and floods, are defined by the NOAA National Centers for Environmental Information (2024) as weather systems producing wind gusts of at least 58 mph, hail one inch or larger in diameter, or tornadic activity. Hailstorms result in widespread damage to crops, vehicles, and rooftops, while tornadoes, known for their violent, rotating columns of air, cause localized but catastrophic destruction to infrastructure and communities. Derechos, long-lived, straight-line windstorms, often lead to power outages and structural damage across vast areas. Flash floods, frequently triggered by intense rainfall during severe storms, overwhelm drainage systems, leading to rapid inundation and significant threats to lives and property. These storms frequently lead to flash flooding and other catastrophic outcomes. Each year, approximately 100,000 thunderstorms occur across the United States, with 10% escalating to severe levels (see National Weather Service (NWS) 2024).

The property insurance sector is under immense pressure due to the increasing frequency and severity of the natural catastrophes. High inflation, shifting population densities toward higher-risk areas, and rising reinsurance costs have stressed traditional insurance models, leading to significant financial challenges for insurers and property owners alike. These systemic pressures not only increase premiums but also affect property valuations and local economies. In high-risk areas where storms and floods are recurrent threats, many homeowners face difficulties securing adequate insurance coverage. Insufficient insurance leaves properties underinsured, slowing recovery efforts and reducing neighborhood property values post-disaster (see New York Times 2024). The impacts of severe storms extend beyond immediate property damage (see Miljkovic et al. 2018). Insights from the National Weather Service (NWS) (2024) highlight significant differences in forecasting capabilities across storm types. For hailstorms, radar and predictive models have improved large-scale forecasting, but precise predictions for specific locations remain a challenge due to their dependence on localized atmospheric dynamics. Tornadoes benefit from advancements in Doppler radar and storm-tracking models, which have enhanced the ability to identify critical conditions like wind shear and instability. However, short lead times and unpredictable formation patterns still pose challenges. Flash floods, often associated with these severe storms, rely on improvements in precipitation monitoring and hydrological modeling, yet their rapid and localized onset makes them difficult to predict accurately. Derechos, being widespread and long-lived windstorms, are the least predictable, with current forecasting systems struggling to determine their trajectories and intensities. The rising cost of insurance affects the feasibility of new developments, determining where infrastructure can be built and at what cost. Unaffordable premiums or a lack of coverage in certain areas disrupt housing markets and expose lenders to increased financial risk (see Office of Financial Research (OFR) 2023). Thus, this financial vulnerability underscores the need for improved severe storm predictions to enhance preparedness. Accurate forecasting enables better risk assessment and allocation of resources, helping insurers, governments, and communities to mitigate the long-term economic and social impacts of these destructive weather events.

1.1. Research Gaps

Despite technological progress, forecasting models face limitations due to incomplete historical data, regional biases, and simplified statistical methods. Historical records, particularly before the 1980s, are often inconsistent, making long-term trend analysis

difficult. Models also struggle to capture the complexity of storm recurrence, especially under evolving climate conditions, and frequently overlook smaller-scale variability. These challenges are compounded by the lack of integration of key environmental variables such as humidity and precipitation (see [González et al. 2020](#); [Zhang et al. 2023](#); [Yang et al. 2024](#)).

The research on the inter-arrival times between severe storms in the United States is limited, particularly when focusing on storms with non-overlapping durations. Non-overlapping durations may indicate a lack of statistical dependence between successive events, which introduces additional complexity in understanding the patterns and frequencies of such events. This gap in the literature creates uncertainty in understanding the patterns and frequencies of such events. While simple statistical models based on the exponential distribution are readily available in the literature, they may not always be appropriate if the inter-arrival times are not exponentially distributed. This raises the question: what alternative models should be considered? Therefore, this study aims to address and close this gap by thoroughly examining the distribution of inter-arrival times between severe storms.

1.2. How Do We Add Value?

To address the gaps in the literature, alternative statistical models are proposed for modeling inter-arrival times between events, enhancing predictive accuracy and reliability. Various theoretical distributions are studied, examining deviations from expected patterns and exploring alternative probability models to better capture observed variations. The following research questions are considered:

- Q1. What is the most suitable probability distribution for modeling inter-arrival times between severe storms in the United States?
- Q2. What is the highest potential financial loss from a single severe storm based on the historical losses?

By answering these research questions we aim to predict the likelihood and timing of the next severe storm. Our approach focuses on extreme occurrences in the tail of the probability distribution. Furthermore, the study estimates expected financial losses associated with these events, offering quantifiable insights into the economic risks posed by severe storms. The insights gained will be crucial for improving insurance and property risk management strategies, providing actionable information to insurers, property developers, policymakers, and other stakeholders to better prepare for and mitigate the financial impacts of severe storms.

The remainder of this paper is structured as follows. Section 2 evaluates existing research on storm recurrence models and highlights key gaps. Section 3 describes the data sources and exploratory data analysis. Section 4 outlines the statistical methods for analyzing storm recurrence with the new proposed approach. Section 5 demonstrates the application of the proposed approach and its practical utility. Section 6 is designed to evaluate recurrence patterns, estimate the probability of the next storm occurrence, and forecast potential impacts, including financial losses. Limitations of the study are discussed in Section 8. Finally, Section 9 provides concluding remarks and opportunities for further work.

2. Literature Review

The literature review, summarized in Table 1, highlights significant advancements in understanding the dynamics of severe storms. Recent studies have employed sophisticated statistical methods and comprehensive datasets to identify patterns, enhance predictive models, and provide actionable insights for mitigating the impacts of severe weather on communities, economies, and infrastructure. A key focus of this research is the distribu-

tion of recurrence times or return intervals between severe storms, which is critical for characterizing and understanding their behavior.

[Santhanam and Kantz \(2008\)](#) explored return intervals between extreme events in long-range correlated systems using simulated Gaussian data. Their findings revealed a dual-distribution behavior, with power-law dominance for short intervals and stretched exponential behavior for longer intervals. Starting with hailstorms and thunderstorm winds, which cause extensive damage to roofs, vehicles, and other property, accurate prediction and mitigation of these events are essential. Thunderstorm winds, in particular, serve as defining metrics for classifying and tracking storm severity.

[Li et al. \(2024\)](#) examined the impacts of hailstorms using data from the Community Collaborative Rain, Hail, and Snow Network (CoCoRaHS), which provided valuable insight into the severity and distribution of hailstorms across a wide geographic area through citizen science observations from 1998 to February 2023. This study utilized Monte Carlo simulations and gamma distribution models to estimate hail-induced roof damage probabilities, demonstrating that impact-resistant roofs reduced damage probabilities by 60% to 98% compared to unrated roofs. While this approach emphasizes uncertainty propagation in physical damage modeling, it does not center on the temporal variability of storm events and their financial implications. Additionally, the authors utilize fragility curves to assess the likelihood of roof damage based on hailstone size, combining physical impact models with uncertainty analysis, without focusing on temporal patterns and clustering of storm events without extending to physical impact modeling.

Similarly, [Van Dijk and Franses \(2003\)](#) analyzed hailstorms and thunderstorm wind events using NOAA's Storm Events Database (1996–2022). By applying the Epidemic-Type Aftershock Sequence (ETAS) model, which is among the most popular stochastic models of seismicity based on a Poisson distribution, they revealed strong clustering of hailstorms in the central U.S., showing that hailstone size has a direct influence on the dynamics and aftermath of hailstorms. The period from 1996 to 2022 was selected because it aligns with the availability and comprehensiveness of the NOAA Storm Events Database, which serves as a robust source for systematically recorded hailstorm and thunderstorm wind events. This period represents a critical timeline during which the database expanded significantly in both its geographic coverage and the detail of its recorded meteorological phenomena. By focusing on this interval, the studies could leverage a large dataset with standardized reporting protocols, enabling more reliable statistical modeling and comparisons. Additionally, this period captures sufficient temporal breadth to observe long-term trends and clustering behaviors, as well as the potential impacts of climate variability on storm dynamics. The inclusion of this timeframe also facilitates the comparison of results with other contemporary analyses, such as [Lo Galbo and Chiodi \(2024\)](#), who examined the same dataset, ensuring methodological consistency and enhancing the validity of cross-study inferences. [Lo Galbo and Chiodi \(2024\)](#) applied the ETAS model to data from the U.S. for the same period to examine spatiotemporal clustering of hailstorms and thunderstorm winds. Their analysis showed that hailstorms tend to occur in close proximity to one another, forming clusters rather than being evenly distributed. Thunderstorm winds also demonstrated limited geographical spread, with their effects confined to relatively smaller areas. Their consistency across different events suggests a stable pattern of behavior.

[Kahn \(2005\)](#) highlighted that windstorms are among the deadliest natural disasters, examining annual deaths from natural disasters between 1980 and 1999 using data from The Emergency Events Database (EM-DAT). The study used zero-inflated negative binomial regressions to analyze the influence of income, geography, and institutional quality on mitigating disaster-related fatalities. The findings indicated that while richer nations expe-

rience as many natural disasters as poorer ones, they have significantly lower fatality rates due to better infrastructure, governance, and response mechanisms, including advanced early warning systems and effective evacuation procedures. In contrast, poorer nations face higher vulnerability due to inadequate infrastructure, dense populations in risk-prone areas, and limited governmental capacity for disaster response.

[Prein and Holland \(2018\)](#) developed a probabilistic hail prediction algorithm using environmental predictors and hail data (1979–2015) across the U.S., Europe, and Australia. The study replicated hail frequency patterns and identified hotspots, such as the U.S. Plains and the lee side of the Andes. On a similar note, [Thorarinsdottir and Gneiting \(2010\)](#) developed a probabilistic wind speed forecasting model using data from meteorological stations in the Pacific Northwest in 2008. The author employed the Ensemble Model Output Statistics (EMOS) technique, which combines multiple linear regression with Gaussian predictive probability density functions to forecast wind speeds. [Richman et al. \(2013\)](#) further highlighted specific atmospheric conditions that indicate a higher likelihood of storm formation. Using principal component analysis (PCA) with varimax rotation, the study analyzed data collected 24 h before severe weather outbreaks in North America. The analysis identified nine to eleven components, such as pressure, moisture, and temperature, that explained variability in severe weather outbreaks like tornadoes, hailstorms, and wind events, demonstrating differences in atmospheric conditions leading to different storm types.

Floods, which are often caused by extreme rainfall, pose significant risks due to their frequency and potential for widespread damage. Understanding the relationship between extreme rainfall and floods is crucial for disaster preparedness, risk management, and policy development. [Dupuis and Trapin \(2023\)](#) examined mesoscale convective systems (MCSs), large organized clusters of thunderstorms that often cause heavy rainfall, and their influence on rainfall in Greater St. Louis, Missouri (1979–2014). Using a mixed-frequency extreme value regression model within the generalized extreme value (GEV) framework, the study found that large clusters of thunderstorms were associated with intense rainfall over short periods, particularly during the afternoon, in July. However, while this study provides valuable insights into rainfall dynamics, it primarily focuses on meteorological factors, leaving broader flood-related considerations unexplored. The interplay between hydrology, urban infrastructure, and socioeconomic conditions is critical to understanding flood severity and impact. This highlights the need for more holistic approaches that integrate these factors into flood research and management.

Tornadoes are among the most violent and unpredictable weather phenomena. [González et al. \(2020\)](#) analyzed tornado reports in the U.S. from 1980 to 2016, focusing on their starting locations and seasonal patterns. Using the spatiotemporal K-function and a studentized permutation test, the study revealed significant seasonal differences in tornado patterns, with stronger clustering observed during the cold season. [Brooks and Dotzek \(2008\)](#) analyzed the spatial distribution and secular changes in severe convective storms globally, focusing on tornadoes, hail, and convective wind events. Using data from the U.S. (1954–2004), the study discovered that tornado intensity distributions could be modeled using Weibull and Rayleigh distributions. It also identified specific environmental conditions, like convective available potential energy (CAPE) and wind shear, as critical predictors of significant severe thunderstorms.

[Elsner et al. \(2016\)](#) evaluated long-term and short-term tornado patterns in the U.S. from 1970 to 2015 using data from NOAA. By employing negative binomial regression and the integrated nested Laplace approximations (INLAs) method for approximate Bayesian inference, the study identified spatial and temporal variations in tornado risks. ENSO (El Niño–Southern Oscillation) was found to significantly influence tornado activity, with El

Niño reducing activity in some areas and increasing it in others. [Potvin et al. \(2022\)](#) further examined tornado frequency in the central U.S. from 1975 to 2018, highlighting reporting biases due to the under-reporting or underestimation of tornado characteristics. Using Bayesian inference with conditional autoregressive models, the study found significant under-reporting of strong tornadoes and a substantial bias correction for weaker tornadoes.

[Yang et al. \(2024\)](#) focused on tornado touchdown data in Kansas from 1950 to 2015, employing a Bayesian zero-inflated Poisson (ZIP) model to estimate touchdown probabilities and identify high-risk areas. Findings indicated that tornado risks were positively correlated with temperature, with higher risks in eastern Kansas compared to western regions. [Daneshvaran and Morden \(2007\)](#) also examined tornado and hail risks in the U.S. using data from the NOAA Storm Prediction Center and Grazulis datasets (1949–2007). By simulating 35,000 years of tornado outbreaks using Monte Carlo simulations and regression analysis, the study found that tornado losses dominate the extreme ends of loss distributions, while hail causes more frequent moderate losses. [Refan et al. \(2020\)](#) examined tornado-related financial losses in Kansas and Oklahoma from 1970 to 2014 using Monte Carlo simulations and negative binomial distribution modeling. The study found that higher tornado frequency and population density in Oklahoma contributed to greater average annual losses compared to Kansas.

The Southeastern United States, often referred to as Dixie Alley, is also a hotspot for tornado activity. [Bradburn \(2016\)](#) analyzed tornado density and return periods in this area using data from 1980 to 2014. By applying kernel density estimation (KDE) and k-means clustering, the study identified specific high-impact areas, particularly in Alabama, Mississippi, and Arkansas. These regions experienced the most intense tornadoes, with high numbers of injuries and fatalities. [Nouri and Devineni \(2022\)](#) examined spatial and temporal changes in large-tornado outbreaks (LTOs) across the U.S. from 1950 to 2019, identifying a southeastward shift in tornado activity and a decrease in spatial dispersion, indicating more localized outbreaks in recent decades.

[Zhang et al. \(2023\)](#) analyzed time trends in tornado-related losses in the U.S. from 1954 to 2018, using statistical models like maximum likelihood estimation (MLE) and the generalized method of moments (GMM). The study found that, after adjusting for inflation, population growth, and economic factors, normalized tornado-related losses have generally declined, though Alabama showed an increasing trend. [Cossette et al. \(2003\)](#) focused on catastrophic events in the U.S. from 1980 to 2001, examining the frequency of events like floods and tornado outbreaks and their associated losses. The study highlighted the correlation between catastrophe intensity and insured losses, emphasizing the difficulty of diversifying risks associated with such events even in large insurance portfolios.

Overall, these studies collectively provide a comprehensive understanding of the dynamics of severe storms, hail, tornadoes, and floods. They have highlighted specific atmospheric conditions, spatial patterns, and clustering behavior, as well as the socioeconomic factors influencing storm impacts and related losses. Such findings are essential for developing predictive models, disaster preparedness plans, and risk management strategies that can mitigate the impacts of severe weather on vulnerable communities and economies.

Table 1. Chronological summary of key studies on severe storm modeling.

Author(s) and Year	Region/Geography	Methods/Models	Main Findings
Cossette et al. (2003)	U.S.	Stochastic ordering	Catastrophe risks need reinsurance, not diversification.
Van Dijk and Franses (2003)	U.S.	Poisson distrib. model	Hailstorms and thunderstorm winds exhibit distinct clustering patterns.
Kahn (2005)	Global	Zero-inflated negative binomial regressions	Wealthier nations experience fewer fatalities.
Daneshvaran and Morden (2007)	U.S.	Monte Carlo simulation, Weibull distrib.	Tornadoes cause severe losses, hail results in moderate damage.
Brooks and Dotzek (2008)	U.S.	Weibull and Rayleigh distrib.	Tornado intensities align with environmental patterns.
Santhanam and Kantz (2008)	Simulated Gaussian data	Power-law and exponential distrib.	Severe storm intervals: power-law short, exponential long.
Thorarinsdottir and Gneiting (2010)	U.S.	Multiple linear regression	Improved wind speed forecasts.
Richman et al. (2013)	North America	Principal component analysis	Moisture, temperature, and pressure changes signal severe storms.
Bradburn (2016)	U.S.	Kernel density estimation	Identified high-risk areas for deadly tornadoes.
Elsner et al. (2016)	U.S.	Negative binomial regression	El Niño shifts tornado risks.
Prein and Holland (2018)	U.S., Europe, Australia	Prediction algorithm	Global hail prediction tool that identifies storm frequencies.
González et al. (2020)	U.S.	Spatiotemporal	Cold-season tornadoes cluster more strongly.
Refan et al. (2020)	U.S.	Monte Carlo simulation	Oklahoma had higher tornado-related losses than Kansas.
Potvin et al. (2022)	U.S.	Bayesian, negative binomial distrib.	Tornadoes were under-reported by a factor of three
Nouri and Devineni (2022)	U.S.	K-medoids clustering, kernel density estimation	Tornado outbreaks are shifting southeastward and are more localized.
Dupuis and Trapin (2023)	U.S.	Generalized extreme value distrib.	Thunderstorms intensify rainfall, especially during July.
Zhang et al. (2023)	U.S.	Maximum likelihood estimation	Tornado-related losses declined nationally by 30%.
Li et al. (2024)	U.S.	Monte Carlo simulations, gamma distrib.	Impact-resistant roofs reduce hail damage by 60–98%.
Yang et al. (2024)	U.S.	Spatiotemporal, Markov chain Monte Carlo	Rising temperatures were linked to increased tornado risks.
Lo Galbo and Chiodi (2024)	U.S.	Maximum likelihood estimation	Hailstorms and thunderstorm winds showed declining clustering.

3. Data

This study utilizes a comprehensive dataset sourced from the National Centers for Environmental Information (NCEI) [NOAA National Centers for Environmental Information \(2024\)](#), cataloging significant billion-dollar disaster events in the United States from 1981 to 2024. The dataset contains a total of 203 observations, each uniquely named, with “severe weather”, and “tornadoes” being among the most frequently mentioned words, emphasizing the recurring nature of these events. However, the events are not further categorized into specific subtypes. Figure 1 shows that severe storms are most prevalent in Texas, followed by Illinois. While they can occur year-round, these events are particularly common in April and May.

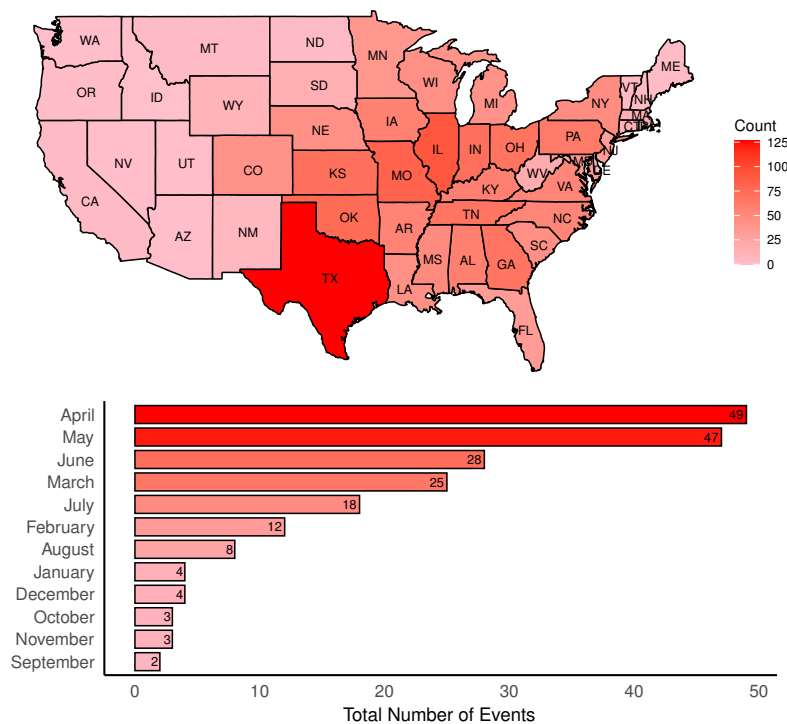


Figure 1. Geographic distribution of severe storm events in the United States (top) and their monthly frequency (bottom) for the period 1981–2024, with months ordered from highest to lowest frequency.

The primary variables chosen for analysis include the type of disaster, the start and end dates of each event, and the Consumer Price Index (CPI)-adjusted financial loss cap. These variables enable a detailed examination of how often severe storms occur, their durations, and the economic impact they impart, though accurately estimating disaster losses remains challenging due to factors such as indirect costs and inconsistencies in reporting. The dataset spans a significant temporal range, with the earliest recorded event occurring on 5 May 1981 and the latest on 13 July 2024, providing over four decades of comprehensive historical records. To analyze the inter-event time between severe storm events, we calculate the difference between the start and end dates for each event. The formula for calculating the inter-arrival time is

$$\text{Inter-event Duration} = (\text{End Date} - \text{Begin Date}) + 1 \tag{1}$$

In this formula, the “Begin Date” and “End Date” represent the respective start and end dates of each severe storm event, ensuring that even single-day events are fully accounted for. The earliest intra-event time was excluded from the analysis as we lacked information about storms preceding the dataset’s starting date, making it impossible to

compute. Using this single dataset from the NCEI allows us to conduct a focused analysis of severe storms over recent decades, highlighting changes in their frequency, duration, and economic impact.

Figure 2 illustrates a clear upward trajectory in the annual occurrence of severe storms, with a pronounced surge in recent years, highlighting a substantial rise in storm frequency over recent decades. Notably, the average annual frequency of storms in the earlier decades (1981–1990) was approximately 0.8 storms per year, compared to an average of 11 storms per year in the most recent decade (2014–2023), representing a more than tenfold increase. Among the years depicted, 2023 stands out with 19 recorded storms, marking it as the highest frequency observed in the dataset and nearly 60% higher than the average of the preceding 10 years. The figure also integrates statistical insights, emphasizing key characteristics of the dataset. The maximum frequency of 19 storms, recorded in 2023, stands out as a significant peak, while the median of 2 storms per year indicates that half the recorded years experienced relatively low storm counts. Interestingly, the mode of one storm per year reflects the most commonly observed annual frequency. This variability reflects the dynamic and cyclical nature of severe weather activity while highlighting the significant escalation in storm frequency in recent decades.

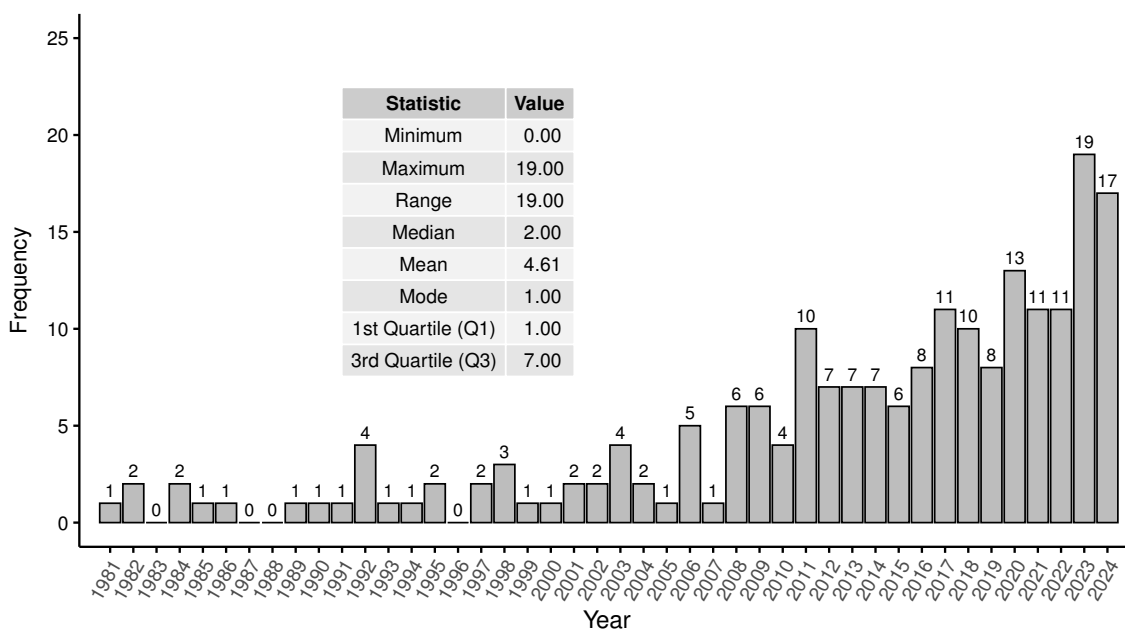


Figure 2. Frequency distribution of severe storm events across years, with descriptive statistics.

Figure 3 shows that no two storms in 2023 occurred on the same date or overlapped in their durations. This was verified by analyzing the start and end dates of each event. The 2023 dataset includes three hail storms (HSs), 15 severe weather (SW) events, and one tornado. This non-overlapping property was observed across the entire dataset. The distinct, non-overlapping boundaries of these events may suggest they can be treated as independent. However, this is not sufficient evidence to claim temporal independence. In order to investigate further the assumption of independence and identically distributed observations, we focus on the distribution of inter-arrival times shown in Figure 4.

Figure 4 illustrates the distribution of inter-event durations for severe storms, presented using both a linear scale and a logarithmic scale for comparison. The distribution is highly right-skewed, with the majority of storm events occurring within short intervals. A pronounced peak is observed within 10 to 50 days. Beyond 50 days, the frequency of inter-event durations declines sharply, with intervals longer than 200 days being relatively

rare. Notable outliers include three extended intervals exceeding 500 days, highlighting significant pauses between major storm occurrences. The longest recorded interval, spanning 1171 days, represents an unusually long gap between the Western Severe Storms and Flooding (February 1986) and the Southern Derecho and Severe Storms (May 1989). The logarithmic transformation of the x-axis addresses the challenges posed by the extreme skewness of the data. The log-transformed scale redistributes inter-event durations to provide greater emphasis on mid-range intervals (10–100 days) that are compressed in the linear representation. The peak density, around 50 days, remains apparent, reinforcing the observation that most storms occur within this timeframe. By compressing larger intervals, the log scale reduces the visual dominance of outliers, such as the 1171-day gap, while still acknowledging their presence. This transformation enhances the visibility of variability across all ranges, particularly for the mid-range durations that are difficult to discern in the linear plot.

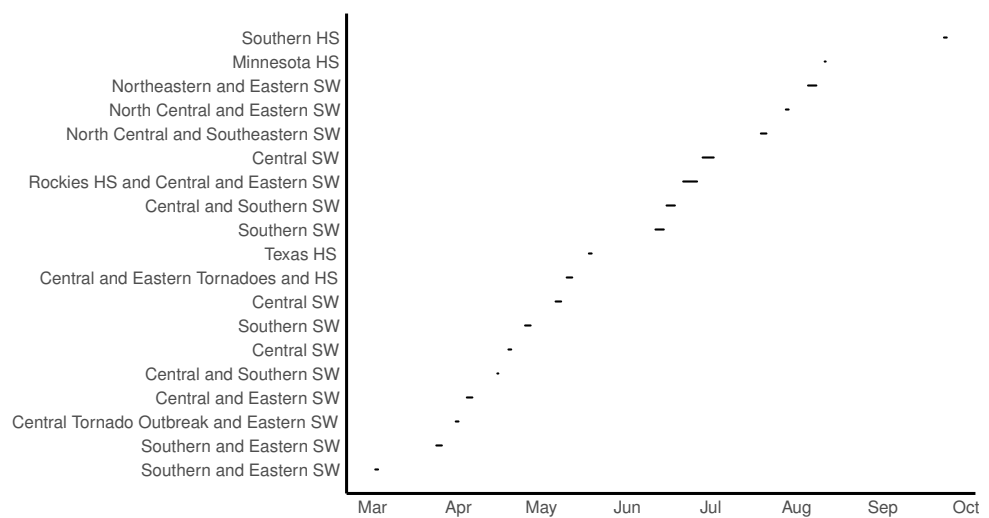


Figure 3. Timeline of severe storm events in 2023 by month, with each short line representing an individual event duration.

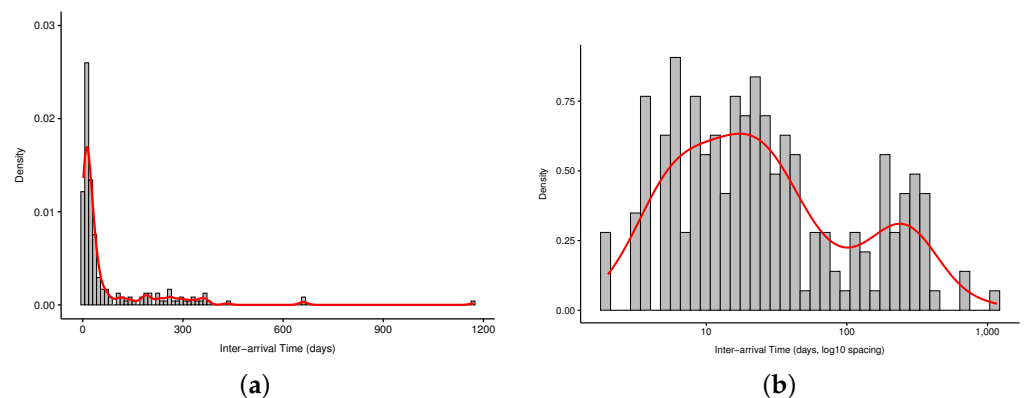


Figure 4. Side-by-side comparison of inter-event duration distributions for severe storms on linear (left) and logarithmic (right) scales. In both plots, histograms are overlaid with density curves to illustrate the distribution of inter-event durations more smoothly. (a) Linear scale. (b) Logarithmic scale.

Together, the linear and log-transformed views in Figure 4 show the complex temporal patterns of severe storms. The linear scale effectively highlights the extremity of the right-skewed distribution, emphasizing the clustering of events within short intervals and the rarity of extended pauses. Meanwhile, the log-transformed scale mitigates the disproportionate influence of outliers, revealing a more balanced view of the data and

emphasizing variability in mid-range intervals. The evidence of multi-modality suggests modeling the inter-arrival time using mixtures to capture heterogeneity in the data, which is the topic of Section 4.

4. Methodology

4.1. Background

In modeling the inter-arrival times, we initially tested several single-component probability distributions—exponential, gamma, Weibull, log-normal, Rayleigh, Gumbel, and generalized Pareto (see Appendix A)—selected for their compatibility with the data's right-skewed, long-tailed characteristics (see Casella and Berger 2002). These distributions are also used to test the assumption of independence in the data. If the rate of the storm occurrence is not constant (e.g., storms are more frequent in certain seasons or under specific weather conditions), the Poisson process assumption breaks down. This can lead to a non-exponential distribution of inter-arrival times. In this section, we explore modeling inter-arrival times using finite mixtures. We apply goodness-of-fit tests, summarized in Appendix B, to show that modeling inter-arrival times using several single-component probability distributions fails. We want to test if inter-arrival times are identically distributed because each one might come from a different component distribution (short intervals vs. long intervals). By allowing multiple distributions to represent these inter-arrival patterns, the mixture model better reflects the natural clustering and variability observed, as detailed in the following subsections.

4.2. Proposed Modeling

To improve the fit for inter-arrival times of storms, we applied a G -component finite mixture model, following the methodology of Blostein and Miljkovic (2019). This approach flexibly combines distributions, such as gamma, log-normal, and Weibull to better capture the complex patterns in recurrence intervals across different storm categories. Although our dataset did not include left-truncated entries, the model's structure is versatile enough to handle varied data patterns.

The model is defined as follows: given a sample $X = (X_1, \dots, X_n)$ of independent and identically distributed inter-arrival time variables, the probability density function is expressed as

$$h(x | \theta) = \sum_{j=1}^G \omega_j g(x | \theta_j) \quad (2)$$

where G is the total number of components in the mixture model, ω_j represents the mixing proportion for each component, constrained such that $\sum_{j=1}^G \omega_j = 1$ and $\omega_j > 0$ for each component j , and $g(x | \theta_j)$ is the probability density function of the j -th component. The parameter vector θ_j is specific to each component, allowing each distribution to capture distinct patterns within the data.

Parameter estimation was performed using the Expectation–Maximization (EM) algorithm proposed by Dempster et al. (1977), which refines initial estimates by iteratively performing expectation (E-step) and maximization (M-step) steps until convergence. This EM-based approach provided robust parameter estimates, thereby enhancing the interpretability and predictive accuracy of the model.

The `1tmix` R package, proposed by Blostein and Miljkovic (2024), was used to fit the G -component model. This package is designed for implementing mixture models with any combination of log-normal, gamma, and Weibull components. Although developed for left-truncated data, we set the truncation parameter to null to suit our dataset. The package also allowed us to calculate component weights and maximum likelihood estimates (MLEs);

the probability density function (PDF), was derived using the MLEs, component weights and cumulative distribution functions (CDFs), facilitating comprehensive model analysis.

To select the best-fitting model configuration, we first used the Akaike information criterion (AIC) proposed by Akaike (1974) and Bayesian information criterion (BIC) proposed by Schwarz (1978), identifying the model with the lowest AIC and BIC values to balance fit accuracy and model complexity. After selecting the best model, we assessed the fit using a series of goodness-of-fit tests, including the Kolmogorov–Smirnov (KS) test, Anderson–Darling (AD) test, and chi-square goodness-of-fit (GOF) test, in addition to a probability–probability (P-P) plot, which is used to compare the CDF of a dataset to the CDF of a theoretical distribution. These tests, which leverage the cumulative distribution function, were instrumental in identifying discrepancies between the observed data and the fitted model. Finally, we plotted the fitted mixture model using the calculated weights and MLEs.

These results were also bench-marked using a non-parametric Kaplan–Meier approach to study the inter-event times between severe storms. This method allows for analyzing the data without assuming a specific parametric distribution, providing flexibility in capturing patterns and trends directly from the observed data.

4.3. Kaplan–Meier Method

To model the likelihood of extended quiet periods between storms, the Kaplan–Meier (KM) estimator, proposed by Kaplan and Meier (1958), was employed. This method calculates the probability that no storm will occur up to a given number of days, known as the survival probability $\hat{S}(t)$, and is defined as

$$\hat{S}(t) = \prod_{t_i \leq t} \left(1 - \frac{d_i}{n_i}\right), \quad (3)$$

where t_i represents the time of the i -th storm event, d_i is the number of storms occurring at t_i , and n_i is the number of intervals at risk just before t_i . The KM estimator provides a robust, non-parametric approach for evaluating inter-arrival times, making it ideal for datasets with variable and clustered storm activity.

The survival function $\hat{S}(t)$ represents the probability that an interval between storms lasts longer than t days. It is related to the CDF $F(t)$, which gives the probability that an interval lasts less than or equal to t days, through the equation

$$\hat{S}(t) = 1 - F(t). \quad (4)$$

Here, $F(t)$ serves as the usual distribution function in this context, quantifying the likelihood of a storm occurring by time t . Conversely, the survival function expresses the probability of no storm occurrence by t , effectively describing the persistence of storm-free intervals. An inverse KM plot visualizes $F(t)$, the cumulative probability that at least one storm has occurred by a given day. This perspective, equivalent to the CDF, offers an intuitive “time-to-first-storm” interpretation. For a more in-depth analysis of the underlying methods and results, refer to Appendix C.

5. Application

In modeling the inter-arrival times of severe storms, a G-component finite mixture model was applied, with the log-normal–log-normal (LL) configuration emerging as the optimal fit based on the lowest AIC and BIC values (see Appendix D, Table A4). This model effectively captures the variability in storm intervals, as demonstrated in Figure 5, where the histogram of observed frequencies aligns closely with the fitted PDF. The density

curve overlays the observed data, accurately reflecting the clustering of shorter inter-arrival times and the tapering off at longer intervals. Figure 5 provides additional validation through a P-P plot, which shows a strong agreement between the empirical CDF and the theoretical CDF predicted by the LL model. The close alignment along the 45-degree line confirms the robustness of the model in representing severe storm recurrence patterns. These results highlight the LL model’s capacity to account for the variability and skewness inherent in inter-arrival times, making it a reliable tool for analyzing and predicting storm recurrence intervals. Confidence in these findings is further reinforced by the consistency of the model’s performance across different statistical measures.

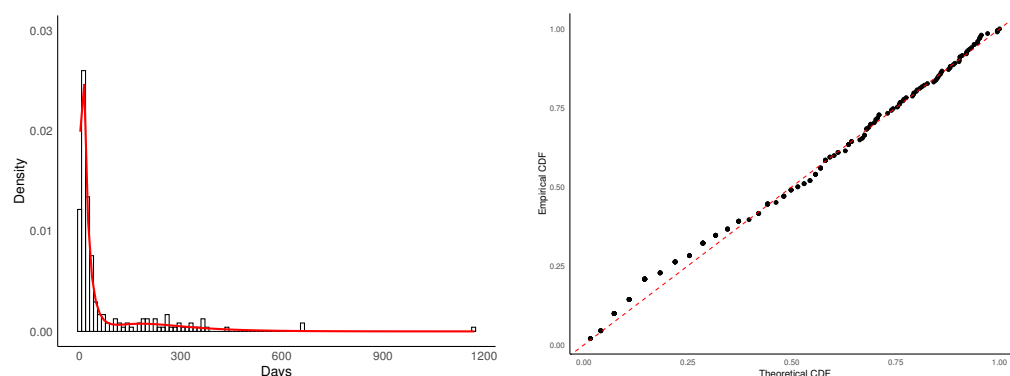


Figure 5. Histogram of the inter-arrival times (left) along with the fitted LL PDF. The P-P plot (right) compares the observed versus theoretical CDFs.

The summary statistics in Table 2 confirm the suitability of the LL mixture model for modeling inter-arrival times of severe storms. The goodness-of-fit tests, including the KS and AD tests, both returned *p*-values above 0.05 (0.43 and 0.78, respectively), indicating no significant deviation between the observed data and the model’s predictions. These results, combined with the low chi-square test statistic (8.54) and its associated *p*-value (0.074), further validate the reliability of the model. The strong alignment of the empirical CDF with the theoretical CDF, as seen in the P-P plot (Figure 5), provides additional support for the model’s robustness.

Table 2. Summary statistics and goodness-of-fit tests for the LL mixture.

	Component 1	Component 2
meanlog	5.53	2.64
sdlog	0.50	0.94
Weights	0.20	0.80
BIC	2011.50	
AIC	1994.96	
Log-likelihood	−992.48	
KS test statistic	0.062	
KS <i>p</i> -value	0.43	
AD test statistic	0.47	
AD <i>p</i> -value	0.78	
χ^2 test statistic	8.54	
χ^2 <i>p</i> -value	0.074	

The LL mixture effectively captures the bimodal nature of storm inter-arrival times, as reflected in the weights assigned to its components: Component 2 accounts for shorter intervals, with a weight of 0.80, while component 1 captures the longer intervals, with a weight of 0.20. The mean log and standard deviation log values for each component

(5.53 and 0.50 for component 1, 2.64 and 0.94 for component 2) highlight the distinct separation between frequent short intervals and the less common extended intervals. By looking closely at the results, the shorter intervals included in component 2 suggest potential temporal dependence, as storms occur in closer succession. Events in component 2 frequently include locations such as Texas, Colorado, and Oklahoma, indicating potential spacial clustering in these states.

6. Simulation

To evaluate recurrence patterns, estimate the probability of the next storm occurrence, and forecast potential impacts, including financial losses, this study conducted a simulation of severe storms' inter-arrival times using the best-fit probabilistic models. Specifically, 1000 simulated samples, each with 1000 iterations, were generated to estimate event occurrence probabilities across selected time thresholds (e.g., 10, 30, 60, 90, 180, and 365 days). These thresholds captured both short- and long-term recurrence patterns, with intervals determined by statistical measures such as the mean and standard deviation (see Appendix D, Table A3).

For each simulated sample, the proportion of inter-arrival times below each threshold was calculated, providing probability estimates for recurrence within specific periods. Confidence intervals of 95% were constructed to assess the reliability of the model, with average probabilities spanning a time range of 15 to 365 days serving as the basis for further analysis.

The simulations, grounded in the LL mixture model, identified as the optimal fit for storm inter-arrival patterns, revealed essential insights into storm recurrence. Figure 6 demonstrates the estimated probabilities of storm recurrence, incorporating the simulated cumulative probability curve, the theoretical curve derived from the LL model, and the inverse KM survival curve, all overlaid on a single plot. Additionally, a zoomed-in inset focuses on the range of 10–90 days, showing the sharp rise in recurrence probability during the initial period and the mean inter-arrival time marked with a vertical dashed red line. The gray shaded area represents the 95% confidence intervals for the estimated probabilities.

The simulation results indicate that the probability of storm occurrence rises sharply in the initial days, stabilizing near 1.0 after approximately 60 days, which aligns closely with the mean inter-arrival time of storms. The narrow confidence intervals within this range further support the reliability of the LL model. The overlay of the KM survival curve and the simulated probability curve highlights the strong agreement between empirical data and model predictions, particularly in the first 90 days, reinforcing the accuracy of the LL model in capturing storm recurrence patterns. These results, as illustrated in Figure 6, emphasize the effectiveness of the LL model in forecasting storm recurrence.

Table 3 below provides detailed simulation probabilities at specific time points, along with their 95% confidence intervals. These probabilities further highlight the sharp increase in storm occurrence likelihood during the initial days, followed by a gradual stabilization over time.

Table 3. Simulation probabilities with 95% confidence intervals.

Days	Simulation Probability	95% CI
10	0.28	(0.25, 0.32)
20	0.52	(0.48, 0.55)
30	0.63	(0.60, 0.66)
90	0.78	(0.77, 0.79)
180	0.85	(0.83, 0.86)

The integration of theoretical modeling, simulated probabilities, and KM curves provides a robust framework for risk assessment associated with the severe storms.

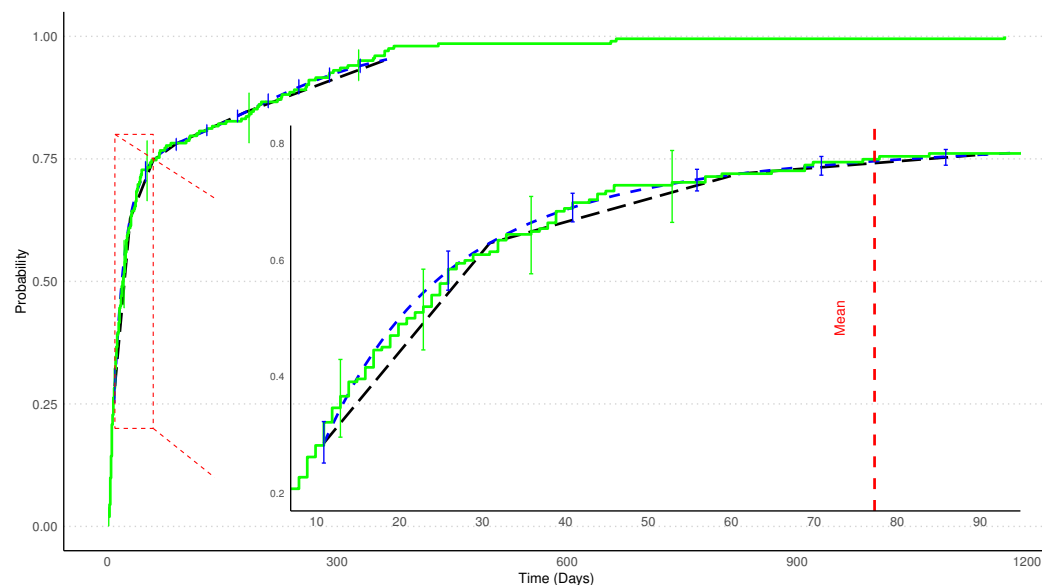


Figure 6. Estimated probabilities of storm recurrence. The plot shows the inverse Kaplan–Meier survival curve (green line) and the simulated cumulative probability curve (blue dashed line), both with 95% confidence intervals represented by vertical lines in matching colors. The theoretical cumulative probability curve from the log-normal–log-normal mixture model is shown as a black dashed line. The vertical red dashed line marks the mean inter-arrival time (in days).

7. Probable Maximum Loss (PML) Analysis

A widely recognized concept in risk analysis and catastrophe modeling, the probable maximum loss (PML) was introduced by [McGuinness \(1969\)](#) and further discussed by [Black and Hurley \(1970\)](#). It provides a monetary estimate of the worst-case scenario loss for a structure or group of structures during a maximum credible event (MCE), such as a significant natural disaster. To construct the PML curve, several calculations were performed to quantify the relationship between event frequency and financial loss, which are explained as follows.

First, the exceedance probability (EP), representing the likelihood of observing losses of a given magnitude or greater in any year, was calculated using the formula

$$EP = \frac{\text{Rank}}{\text{Total Number of Events} + 1} \quad (5)$$

Here, the rank represents the position of an event in the sorted list of storm events, ordered from the largest to the smallest severity of losses. The severity of losses is expressed as adjusted cost using a Consumer Price Index (CPI-adjusted). In our data, the total number of events is 203, and the addition of one ensures the probability remains below one even for the largest event. For example, the largest event (rank 1) will have an EP slightly less than 1, reflecting the uncertainty associated with finite data.

Using the exceedance probability, the return period (T), which represents the average recurrence interval for events of a given magnitude, was calculated as

$$T = \frac{1}{EP}. \quad (6)$$

The return period, expressed in days, indicates how often an event of a particular size might be expected to occur on average. For example, an event with an exceedance probability of 0.005 would have a return period of 200 days, meaning it is expected to occur approximately once every 200 days.

The financial loss associated with each return period was calculated based on the CPI-adjusted cost of the storm event, converted into billions of USD for clarity. The conversion is given by

$$\text{Loss in Billions} = \frac{\text{CPI-Adjusted Cost}}{1000}. \quad (7)$$

This step adjusts all costs for inflation, ensuring consistency across years, and expresses losses in a simplified monetary unit for better readability.

To annotate key points on the PML curve, specific return periods were selected (e.g., 20.3, 50.8, 101.5, and 203 days). Events closest to these return periods were identified by minimizing the difference between their calculated return period and the target values. The annotations include both the return period and the corresponding PML percentage, calculated as

$$\text{PML (\%)} = \frac{1}{T} \times 100. \quad (8)$$

This highlights the likelihood of observing such events as a percentage. For example, a return period of 203 days corresponds to an exceedance probability of approximately 0.005 (0.5%), representing the chance of experiencing a loss of this magnitude or greater in any given day.

The relationship between return periods and losses forms the basis of the PML curve. This curve provides a quantitative visualization of the increasing financial impact of rarer, more severe events. Selected return periods and their corresponding losses and PML percentages are summarized in Table 4.

Figure 7 illustrates the PML curve, which captures the nonlinear relationship between return periods and financial losses. The red line represents the overall trend, reflecting the increasing losses associated with less frequent, higher-severity storm events. Blue markers denote key return periods, providing actionable benchmarks for decision making.

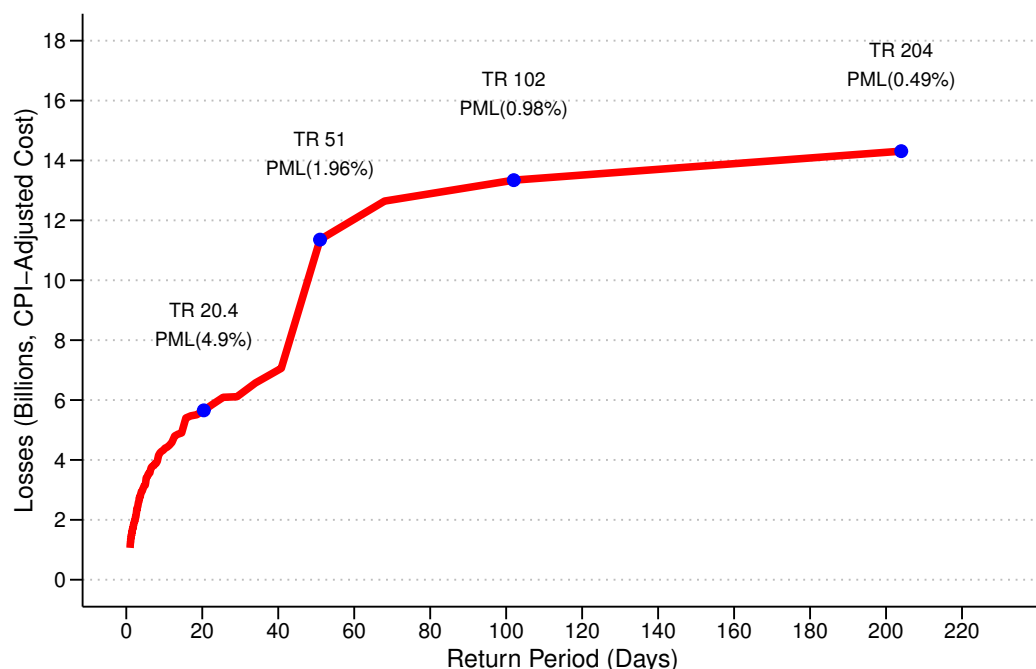


Figure 7. Probable maximum loss (PML) curve with key return period markers.

The PML curve reveals a steep increase in financial losses with longer return periods. For instance, a return period of 20.3 days corresponds to a loss of USD 5.66 billion, with a PML percentage of 4.93%, while a return period of 203 days is associated with a loss of USD

14.31 billion, with a PML of 0.49%. These findings underscore the significant financial risks posed by rare but severe catastrophic events, demonstrating the necessity of probabilistic modeling for comprehensive disaster risk management.

Table 4. Loss estimates and PML percentages for selected return periods.

Return Period (Days)	Loss (Billions, USD)	PML (%)
20.3	5.66	4.93
50.8	11.36	1.97
101.5	13.34	0.99
203.0	14.31	0.49

8. Limitations

Several limitations of this study are discussed as follows, based on the current analysis and understanding of the data and methods used. In this study, we utilized BIC as the primary criterion for model selection, as it is a widely accepted approach in finite mixture modeling. While additional methods such as cross-validation, posterior predictive checks, and out-of-sample validation are recognized as valuable for assessing predictive accuracy, the relatively small sample size limited our ability to implement these techniques robustly. Predictive validation methods often require splitting the dataset into training and testing subsets, which can reduce the effective sample size for model estimation. With a limited dataset, this could lead to unstable or unreliable estimates. Future work may address this limitation by collecting additional data or accessing independent datasets. A larger sample size will facilitate more rigorous validation techniques, including holdout validation and cross-validation, to further ensure the robustness and predictive accuracy of the model.

The EM algorithm, while effective for fitting finite mixture models, is sensitive to outliers due to its reliance on likelihood maximization. In our storm data, which include rare but extreme events, outliers may have a disproportionate influence on parameter estimates and component assignments. However, these are legitimate data points and should not be excluded from the data. To mitigate this, we believe that a robust initialization in the EM algorithm reduces the impact of outliers. However, one can explore different component distributions (i.e., Burr, inverse Burr, etc.) beyond those used in our study in order to improve the fit in the tail.

The assumption of statistical independence between events is a major limiting factor in this study. Future work may focus on distinguishing among types of disasters and limitations of statistical approaches due to the differences. Also, forcing functions for different types of flood, hail, tornado, or other disasters are different, although they are mostly weather-induced.

9. Conclusions and Future Work

In this study, we introduced a comprehensive statistical approach for analyzing the recurrence patterns of severe storms in the United States from 1981 to 2024. By leveraging a log-normal–log-normal mixture model, we addressed the complexities of storm inter-arrival times, capturing both frequent, closely spaced events and extended quiet periods with high precision. Analyzing the observations within each component of the mixture allowed us to study temporal dependencies associated with specific regions where these events occurred. The Expectation–Maximization (EM) algorithm facilitated robust parameter estimation, and the reliability of the model was validated through goodness-of-fit tests. Unlike traditional methods, the proposed model accounts for nuanced variations in inter-event durations, thereby enhancing predictive accuracy. Additionally, the incorporation

of a Kaplan–Meier analysis enriched the study by evaluating storm-free intervals non-parametrically, providing a useful benchmark against the parametric results.

A simulation study was implemented to validate the empirical findings of the log-normal–log-normal mixture model. Specifically, 1000 simulated samples, each with 1000 iterations, were generated to estimate event occurrence probabilities across various thresholds (ranging from 10 to 365 days) with their 95% confidence intervals. The results indicated that the probability of storm occurrence rises sharply in the initial days, stabilizing near 1 after approximately 60 days. This pattern aligns closely with the observed mean inter-arrival time of storms. Both parametric and non-parametric (Kaplan–Meier) approaches highlighted a consistent agreement in the results.

Based on the historical data, a PML curve is constructed for severe storms, providing valuable insights into potential financial risks associated with these events. The analysis estimates that a period of 20.3 days between storms corresponds to a loss of USD 5.66 billion, while a return period of 203 days (less than 6 months) is associated with a loss of USD 14 billion. These findings are crucial not only for risk managers and actuaries working in the insurance and reinsurance industries, who rely on accurate loss projections to set premiums and reserves, but also for government agencies and policymakers responsible for disaster preparedness and financial risk mitigation strategies. Understanding these loss estimates helps ensure more effective decision making, resource allocation, and resilience planning in the face of severe storms.

While this study focuses on modeling the inter-arrival times of severe storms, applying similar statistical approaches to flood events presents unique challenges. Floods are complex phenomena influenced by hydrologic factors, watershed characteristics, and precipitation patterns, often resulting in clustering and dependencies not captured by simple statistical distributions. For instance, methods such as those outlined in Bulletin 17C (England et al. 2018) emphasize the use of hydrologic models and advanced statistical techniques like the Expected Moments Algorithm (EMA) to address data censoring, regional skew, and non-stationary trends in flood data. Incorporating such approaches, which are well established in flood frequency analysis, could improve the applicability of statistical models to flood-related inter-arrival studies. Additionally, the assumption of independence inherent in many statistical models may not hold for flood events, where antecedent conditions and spatial dependencies play a significant role. Future work could expand on this study's findings by integrating hydrologic and climate-based variables into the modeling of storm and flood inter-arrival times. Drawing from methodologies in Bulletin 17C (England et al. 2018), such as the EMA and regional skew adjustments, would provide a more comprehensive framework for analyzing the complex dependencies and clustering behaviors characteristic of flood events.

Finally, the results of this study are based on data collected from storms that caused at least USD 1 billion in losses. While this approach highlights the most economically significant events, it excludes smaller-scale storms that may exhibit different recurrence patterns and levels of dependence. Expanding the dataset to include storms with losses below USD 1 billion could provide a more comprehensive understanding of storm dynamics, particularly regarding whether the assumption of independence holds across events of varying scales. Future research should focus on assessing whether the log-normal–log-normal mixture model remains appropriate for modeling inter-arrival times with this broader dataset. Additionally, the inclusion of smaller-scale storms may reveal clustering or dependencies that are less evident in high-cost events. Exploring alternative models and distributional assumptions would ensure robust predictions and offer insights into storm recurrence across diverse storm types and scales.

Author Contributions: Writing—original draft preparation, I.V. and writing—review and editing, T.M.; formal analysis and investigation, I.V.; data curation, I.V.; Conceptualization and supervision, T.M. All authors have read and agreed to the published version of the manuscript.

Funding: This research received no external funding.

Data Availability Statement: <https://www.ncei.noaa.gov/access/billions/> (accessed on 15 September 2024).

Acknowledgments: The authors wish to thank the Editor-in-Chief, the Associate Editor and two anonymous reviewers for their many helpful and insightful comments and suggestions that greatly improved the paper.

Conflicts of Interest: The authors declare no conflicts of interest.

Appendix A. Distributions Used in Analysis

The distributions used in the analysis offer different characteristics that make them suitable for time-to-event modeling.

Rayleigh Distribution: The Rayleigh distribution is often used for modeling time-to-event data, especially when the variance increases over time. The distribution is defined as

$$f(x|\sigma) = \frac{x}{\sigma^2} e^{-\frac{x^2}{2\sigma^2}},$$

where σ is the scale parameter, and $\sigma > 0$. The range of x is $[0, \infty)$.

Exponential Distribution: Commonly used for modeling the time between independent events, the exponential distribution assumes a “memoryless” property, which is useful for disaster recurrence analysis. It is defined as

$$f(x|\lambda) = \lambda e^{-\lambda x},$$

where λ is the rate parameter, and $\lambda > 0$. The range of x is $[0, \infty)$.

Gamma Distribution: The gamma distribution is flexible and can model the time until multiple events occur. It is defined as

$$f(x|\alpha, \theta) = \frac{\theta^\alpha}{\Gamma(\alpha)} x^{\alpha-1} e^{-x\theta},$$

where α is the shape parameter ($\alpha > 0$) and θ is the scale parameter ($\theta > 0$). The range of x is $[0, \infty)$.

Weibull Distribution: The Weibull distribution is particularly suited for analyzing time-to-event data where hazard rates change over time. Its density function is

$$f(x|\lambda, k) = \frac{k}{\lambda} \left(\frac{x}{\lambda}\right)^{k-1} e^{-\left(\frac{x}{\lambda}\right)^k},$$

where λ is the scale parameter ($\lambda > 0$) and k is the shape parameter ($k > 0$). The range of x is $[0, \infty)$.

Generalized Pareto Distribution (GPD): The GPD is used in extreme value theory to model the tails of distributions, which is important when considering rare, extreme disasters. Its density function is

$$f(x|\xi, \sigma, \mu) = \frac{1}{\sigma} \left(1 + \frac{\xi(x - \mu)}{\sigma}\right)^{-\frac{1}{\xi}-1},$$

where ξ is the shape parameter ($\xi > -\sigma/(x - \mu)$), σ is the scale parameter ($\sigma > 0$), and μ is the location parameter ($\mu \in \mathbb{R}$). The range of x is $[\mu, \infty)$ if $\xi \geq 0$, and $[\mu, \mu - \sigma/\xi)$ if $\xi < 0$.

Log-Normal Distribution: Used to model data that are positively skewed, the log-normal distribution is suitable when the underlying data represent multiplicative processes. Its density function is

$$f(x|\mu, \sigma) = \frac{1}{x\sigma\sqrt{2\pi}} e^{-\frac{(\ln x - \mu)^2}{2\sigma^2}},$$

where μ and σ are the mean and standard deviation of the logarithmic values of x , with $\sigma > 0$. The range of x is $[0, \infty)$.

Gumbel Distribution: The Gumbel distribution is often used for modeling the distribution of the maximum or minimum of a number of samples. It is defined as

$$f(x|\mu, \beta) = \frac{1}{\beta} e^{-\left(\frac{x-\mu}{\beta}\right)} e^{-e^{-\left(\frac{x-\mu}{\beta}\right)}},$$

where μ is the location parameter ($\mu \in \mathbb{R}$) and β is the scale parameter ($\beta > 0$). The range of x is $(-\infty, \infty)$.

Mixture of Two Log-Normal Distributions: A mixture of two log-normal distributions is often used to model data with two distinct subpopulations, each following a log-normal distribution. The probability density function (PDF) of the mixture is given by

$$f(x|w_1, \mu_1, \sigma_1, \mu_2, \sigma_2) = w_1 \cdot \frac{1}{x\sigma_1\sqrt{2\pi}} e^{-\frac{(\ln(x)-\mu_1)^2}{2\sigma_1^2}} + (1 - w_1) \cdot \frac{1}{x\sigma_2\sqrt{2\pi}} e^{-\frac{(\ln(x)-\mu_2)^2}{2\sigma_2^2}},$$

where

- $w_1 \in [0, 1]$: The weight of the first log-normal component.
- $\mu_1, \mu_2 \in \mathbb{R}$: The means of the logarithms of the two log-normal components.
- $\sigma_1, \sigma_2 > 0$: The standard deviations of the logarithms of the two log-normal components.
- $x \in (0, \infty)$: The random variable being modeled.

The first term corresponds to the first log-normal component, scaled by its weight w_1 , and the second term corresponds to the second log-normal component, scaled by $1 - w_1$.

Appendix B. Goodness-of-Fit Tests Used in Analysis

To determine the best-fitting distributions for the inter-event durations, three goodness-of-fit (GOF) tests were applied: The Kolmogorov–Smirnov test, the Chi-square goodness-of-fit test, and the Anderson–Darling test.

Kolmogorov–Smirnov Test (KS Test): The KS test compares the empirical distribution function of the data with the cumulative distribution function of the theoretical model. The test statistic is

$$D = \sup_x |F_n(x) - F(x)|,$$

where $F_n(x)$ is the empirical CDF and $F(x)$ is the theoretical CDF. The p -values for this test indicate how well the theoretical distribution fits the observed data.

Chi-square Goodness-of-Fit Test: The chi-square test compares the observed and expected frequencies of disaster durations under each theoretical distribution. It is calculated as

$$\chi^2 = \sum \frac{(O_i - E_i)^2}{E_i}$$

where O_i is the observed frequency in the i -th category and E_i is the expected frequency based on the theoretical distribution.

Anderson–Darling Test: The Anderson–Darling test places more emphasis on the tails of the distribution, making it more sensitive to extreme values. The test statistic is

$$A^2 = -n - \frac{1}{n} \sum_{i=1}^n (2i - 1) [\ln(F(X_i)) + \ln(1 - F(X_{n+1-i}))]$$

where n is the sample size, X_i is the ordered data points, and $F(X_i)$ is the cumulative distribution function.

Appendix C. Kaplan–Meier Supplementary Analysis

The KM survival analysis, presented in Figure A1 and Table A1, reveals that by day 100, the cumulative probability of experiencing a storm exceeds 90%, highlighting the frequent and clustered nature of storm events. The rapid decline in survival probability underscores the quick recurrence of storms, with minimal time between events. The shaded region in Figure A1 represents the 95% confidence intervals, indicating the bounds of uncertainty around the estimates. At shorter inter-arrival times, the intervals are narrower due to the high density of data, while at longer intervals, they widen as data become sparse, reflecting increased uncertainty. This variability emphasizes the unpredictability of extended storm-free periods.

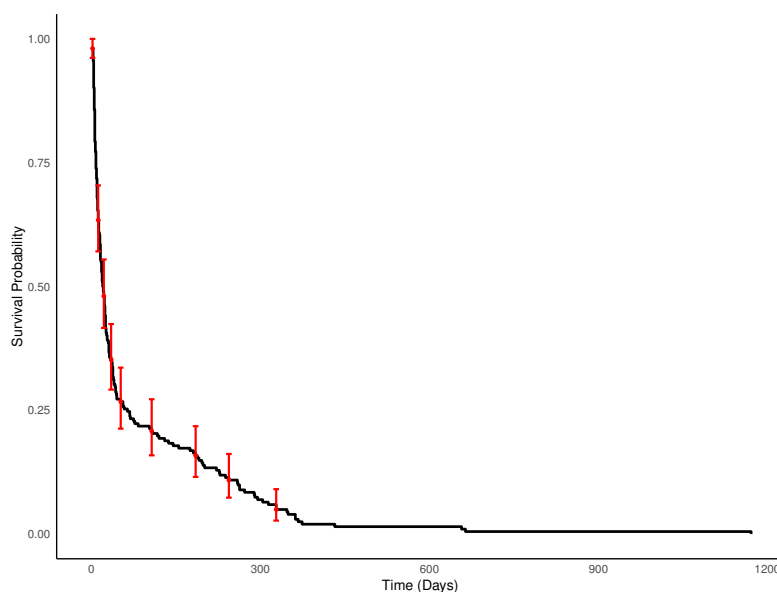


Figure A1. The KM survival curve, depicting the probability of time between severe storm events with 95% confidence intervals, represented by red vertical error bars.

Table A1. Kaplan–Meier survival analysis summary.

Characteristic	Value
Number at risk at 1 year	6
Number of events at 1 year	196
1-Year survival probability	2.97% (95% CI: 1.35%, 6.53%)
Median survival (days)	20.5 (95% CI: 16, 25)

The analysis provides significant insights. The median survival time—indicating when 50% of intervals have experienced a storm—is just 20.5 days, underscoring the brief gaps between storm occurrences. Additionally, the 1-year survival probability, or the likelihood of not experiencing a storm within 365 days, is extremely low at 2.97%.

Appendix D. Tables and Figures

Table A2. Goodness-of-fit results for single-component probability distributions.

Distribution	MLEs	χ^2 Statistic	χ^2 p-Value	AD Statistic	AD p-Value
Exponential	$\lambda = 0.013$	152.81	0	9.50	<0.001
Gamma	$\alpha = 0.31, \beta = 0.0040$	109.55	<0.001	9.32	<0.001
Weibull	$\alpha = 0.67, \beta = 53.86$	92.72	<0.001	7.43	<0.001
Log-normal	$\mu = 3.23, \sigma = 1.45$	49.80	<0.001	3.14	<0.001
GPD	$\xi = -0.1, \sigma = 30, \mu = 0$	136.32	0	1.040	0.0095
Rayleigh	$\sigma = 111.51$	>200	0	>200	0
Gumbel	$\mu = 31.04, \sigma = 59.01$	>200	0	26.12	0

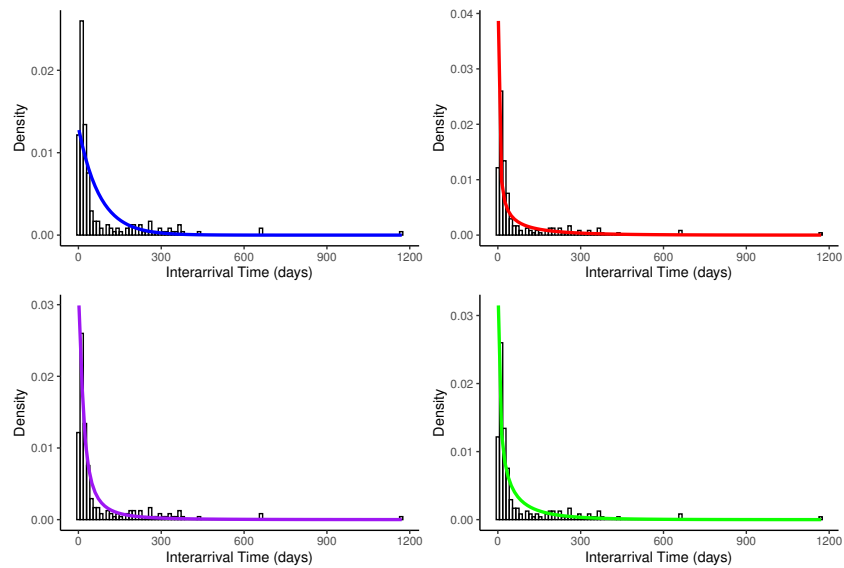


Figure A2. Fitting different distributions to the inter-arrival time: Exponential (top left), gamma (top right), log-normal (bottom right), Weibull (bottom left).

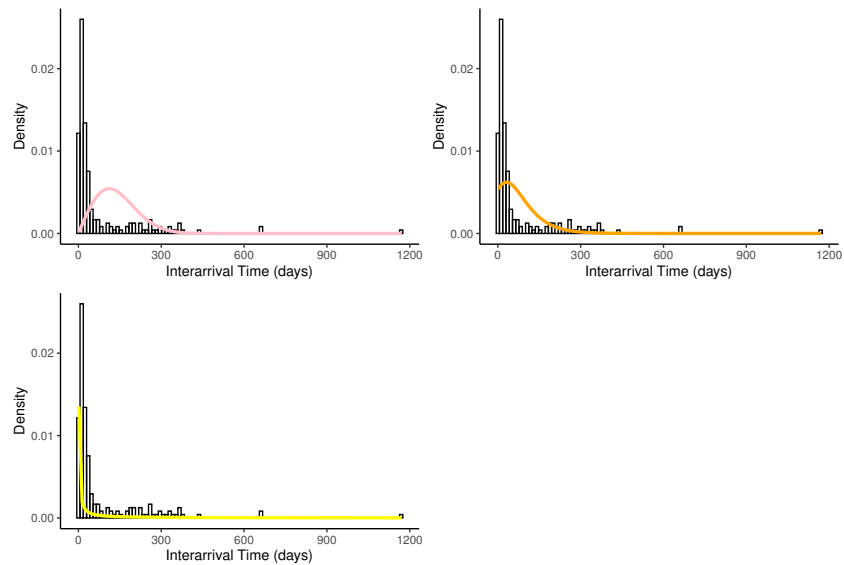


Figure A3. Fitting different distributions to the inter-arrival time: Rayleigh (top left), Gumbel (top right), generalized Pareto (bottom left).

Table A3. Summary statistics for severe storm events across all years (1981 to 2024).

Statistic	Value
Minimum	2.00
1st Quartile	8.00
Median	20.50
Mean	76.41
3rd Quartile	62.50
Maximum	1171.00
First Standard Deviation	138.29

Table A4. Summary results for mixture models. * NLL (negative log-likelihood). ** ΔAIC and ** ΔBIC represent differences in AIC and BIC relative to the best model (the one with the lowest AIC or BIC).

Model	Component G1	Component G2	Component G3	NLL *	AIC	BIC	ΔAIC **	ΔBIC **
G	Gamma	NA	NA	−1041.2321	2086.464	2093.061	107.2331	95.0182
L	Log-normal	NA	NA	−1007.1072	2018.214	2024.811	38.9834	26.7684
W	Weibull	NA	NA	−1030.2376	2064.475	2071.072	85.2442	73.0292
GG	Gamma	Gamma	NA	−991.6013	1993.203	2009.694	13.9715	11.6515
GL	Gamma	Log-normal	NA	−987.5380	1985.076	2001.568	5.8449	3.5250
GW	Gamma	Weibull	NA	−991.9437	1993.887	2010.379	14.6563	12.3363
LL	Log-normal	Log-normal	NA	−985.7755	1981.551	1998.043	2.3200	0.0000
LW	Log-normal	Weibull	NA	−992.9091	1995.818	2012.310	16.5870	14.2671
WW	Weibull	Weibull	NA	−993.7595	1997.519	2014.011	18.2879	15.9680
GGG	Gamma	Gamma	Gamma	−983.1525	1982.305	2008.692	3.0739	10.6489
GGL	Gamma	Gamma	Log-normal	−983.1572	1982.314	2008.701	3.0833	10.6583
GGW	Gamma	Gamma	Weibull	−983.9881	1983.976	2010.363	4.7452	12.3202
GLL	Gamma	Log-normal	Log-normal	−981.7309	1979.462	2005.848	0.2308	7.8058
GLW	Gamma	Log-normal	Weibull	−983.8550	1983.710	2010.096	4.4788	12.0538
GWW	Gamma	Weibull	Weibull	−984.1801	1984.360	2010.747	5.1291	12.7041
LLL	Log-normal	Log-normal	Log-normal	−981.6155	1979.231	2005.618	0.0000	7.5750
LLW	Log-normal	Log-normal	Weibull	−982.9170	1981.834	2008.221	2.6030	10.1780
LWW	Log-normal	Weibull	Weibull	−984.3425	1984.685	2011.072	5.4540	13.0290
WWW	Weibull	Weibull	Weibull	−985.3793	1986.759	2013.145	7.5276	15.1026

References

Akaike, Hirotugu. 1974. A New Look at the Statistical Model Identification. *IEEE Transactions on Automatic Control* 19: 716–23. [CrossRef]

Black, Edward B., and Robert L. Hurley. 1970. Is “Probable Maximum Loss” (PML) a Useful Concept? *Assurances* 38: 169–88. [CrossRef]

Blostein, Martin, and Tatjana Miljkovic. 2019. On Modeling Left-Truncated Loss Data Using Mixtures of Distributions. *Insurance Mathematics and Economics* 85: 35–46. [CrossRef]

Blostein, Martin, and Tatjana Miljkovic. 2024. Itmix: Mixture Models for Lifetime Data. Available online: <https://CRAN.R-project.org/package=ltmix> (accessed on 15 September 2024).

Bradburn, Michelle. 2016. Tornado Density and Return Periods in the Southeastern United States: Communicating Risk and Vulnerability at the Regional and State Levels. Master’s thesis, Electronic theses and dissertations, East Tennessee State University, Johnson City, TN, USA.

Brooks, Harold E., and Nikolai Dotzek. 2008. The Spatial Distribution of Severe Convective Storms and an Analysis of Their Secular Changes. In *Climate Extremes and Society*. Cambridge: Cambridge University Press, vol. 35, p. 53.

Casella, George, and Roger L. Berger. 2002. *Statistical Inference*, 2nd ed. Chapman & Hall/CRC Texts in Statistical Science. Boca Raton: CRC Press.

Cossette, Hélène, Thierry Duchesne, and Étienne Marceau. 2003. Modeling Catastrophes and Their Impact on Insurance Portfolios. *North American Actuarial Journal* 7: 1–22. [CrossRef]

Daneshvaran, Siamak, and Robert E. Morden. 2007. Tornado Risk Analysis in the United States. *The Journal of Risk Finance* 8: 97–111. [CrossRef]

Dempster, Arthur P., Nan M. Laird, and Donald B. Rubin. 1977. Maximum Likelihood from Incomplete Data Via the EM-Algorithm. *Journal of the Royal Statistical Society: Series B (Methodological)* 39: 22. [CrossRef]

Dupuis, Debbie J., and Luca Trapin. 2023. Mixed-Frequency Extreme Value Regression: Estimating the Effect of Mesoscale Convective Systems on Extreme Rainfall Intensity. *The Annals of Applied Statistics* 17: 1398–418. [CrossRef]

- Elsner, James B., Thomas H. Jagger, and Tyler Fricker. 2016. Statistical Models for Tornado Climatology: Long and Short-Term Views. *PLoS ONE* 11: e0166895. [CrossRef] [PubMed]
- England, John F., Jr., Timothy A. Cohn, Beth A. Faber, Jerry R. Stedinger, Wilbert O. Thomas, Jr., Andrea G. Veilleux, Julie E. Kiang, and Robert R. Mason, Jr. 2018. *Guidelines for Determining Flood Flow Frequency—Bulletin 17C*. Reston: U.S. Geological Survey.
- González, Jonatan A., Ute Hahn, and Jorge Mateu. 2020. Analysis of Tornado Reports Through Replicated Spatiotemporal Point Patterns. *Journal of the Royal Statistical Society: Series C (Applied Statistics)* 69: 3–23. [CrossRef]
- Kaas, Rob, Marc Goovaerts, Jan Dhaene, and Michel Denuit. 2008. *Modern Actuarial Risk Theory: Using R*, 3rd ed. Berlin and Heidelberg: Springer. [CrossRef]
- Kahn, Matthew E. 2005. The Death Toll from Natural Disasters: The Role of Income, Geography, and Institutions. *Review of Economics and Statistics* 87: 271–84. [CrossRef]
- Kaplan, Edward L., and Paul Meier. 1958. Nonparametric Estimation from Incomplete Observations. *Journal of the American Statistical Association* 53: 457–81. [CrossRef]
- Klugman, Stuart A., Harry H. Panjer, and Gordon E. Willmot. 2019. *Loss Models: From Data to Decisions*, 5th ed. Hoboken: John Wiley & Sons.
- Li, Yao, Keith Porter, and Katsuchihiro Goda. 2024. Hail Hazard Modeling with Uncertainty Analysis and Roof Damage Estimation of Residential Buildings in North America. *International Journal of Disaster Risk Reduction* 113: 104853. [CrossRef]
- Lo Galbo, Giada, and Marcello Chiodi. 2024. Severe Convective Storms' Reproduction: Empirical Analysis from the Marked Self-Exciting Point Processes Point of View. *Environmental and Ecological Statistics* 31: 409–31. [CrossRef]
- McGuinness, John S. 1969. Is "Probable Maximum Loss" (PML) a Useful Concept? *Proceedings of the Casualty Actuarial Society* 56: 31–40.
- Miljkovic, Tatjana, Dragan Miljkovic, and Karsten Maurer. 2018. Examining the impact on mortality arising from climate change: Important findings for the insurance industry. *European Actuarial Journal* 8: 363–81. [CrossRef]
- NAIC. 2023. Property & Casualty Insurance Industry. Available online: <https://content.naic.org> (accessed on 15 September 2024).
- National Weather Service (NWS). 2024. Lightning Science and Safety. Available online: <https://www.weather.gov/safety/lightning-science-thunder> (accessed on 27 August 2024).
- New York Times. 2024. Home Insurance and Climate Change. Available online: <https://www.nytimes.com/interactive/2024/07/08/climate/home-insurance-climate-change.html> (accessed on 15 September 2024).
- NOAA National Centers for Environmental Information. 2024. U.S. Billion-Dollar Weather and Climate Disasters. Available online: <https://www.ncei.noaa.gov/access/billions/> (accessed on 1 September 2024).
- Nouri, Niloufar, and Naresh Devineni. 2022. Examining the Changes in the Spatial Manifestation and the Rate of Arrival of Large Tornado Outbreaks. *Environmental Research Communications* 4: 10. [CrossRef]
- Office of Financial Research (OFR). 2023. Property Insurance Market and Financial Stability. Available online: <https://www.financialresearch.gov/the-ofr-blog> (accessed on 1 October 2024).
- Potvin, Corey K., Chris Broyles, Patrick S. Skinner, and Harold E. Brooks. 2022. Improving Estimates of US Tornado Frequency by Accounting for Unreported and Underrated Tornadoes. *Journal of Applied Meteorology and Climatology* 61: 909–30. [CrossRef]
- Prein, Andreas F., and Greg J. Holland. 2018. Global Estimates of Damaging Hail Hazard. *Weather and Climate Extremes* 22: 10–23. [CrossRef]
- Refan, Maryam, Djordje Romanic, Dan Parvu, and Gero Michel. 2020. Tornado Loss Model of Oklahoma and Kansas, United States, Based on the Historical Tornado Data and Monte Carlo Simulation. *International Journal of Disaster Risk Reduction* 43: 16. [CrossRef]
- Richman, Michael B., Andrew E. Mercer, Lance M. Leslie, Charles A. Doswell, III, and Chad M. Shafer. 2013. High Dimensional Dataset Compression Using Principal Components. *Open Journal of Statistics* 3: 356–66. [CrossRef]
- Santhanam, M. S., and Holger Kantz. 2008. Return Interval Distribution of Extreme Events and Long-Term Memory. *Physical Review E—Statistical, Nonlinear, and Soft Matter Physics* 78: 9. [CrossRef]
- Schwarz, Gideon. 1978. Estimating the Dimension of a Model. *The Annals of Statistics* 6: 461–64. [CrossRef]
- Thorarindottir, Thordis L., and Tilmann Gneiting. 2010. Probabilistic Forecasts of Wind Speed: Ensemble Model Output Statistics by Using Heteroscedastic Censored Regression. *Journal of the Royal Statistical Society: Series A (Statistics in Society)* 173: 371–88. [CrossRef]
- Van Dijk, Dick, and Philip Hans Franses. 2003. Selecting a Nonlinear Time Series Model Using Weighted Tests of Equal Forecast Accuracy. *Oxford Bulletin of Economics and Statistics* 65: 727–44. [CrossRef]
- Yang, Hong-Ding, Audrey Chang, Wei-Wen Hsu, and Chun-Shu Chen. 2024. A Zero-Inflated Model for Spatiotemporal Count Data with Extra Zeros: Application to 1950–2015 Tornado Data in Kansas. *Environmental and Ecological Statistics* 31: 1–25. [CrossRef]
- Zhang, Jinhui, Stefan Trück, Chi Truong, and David Pitt. 2023. Time Trends in Losses from Major Tornadoes in the United States. *Weather and Climate Extremes* 41: 14. [CrossRef]

Disclaimer/Publisher's Note: The statements, opinions and data contained in all publications are solely those of the individual author(s) and contributor(s) and not of MDPI and/or the editor(s). MDPI and/or the editor(s) disclaim responsibility for any injury to people or property resulting from any ideas, methods, instructions or products referred to in the content.